J. Phys. D: Appl. Phys. **46** (2013) 035103 (6pp) doi:10.1088/0022-3727/46/3/035103

Enhanced photocatalytic performance: a β-Bi_2O_3 thin film by nanoporous surface

Xin Yang, Xiaojuan Lian, Shangjun Liu, Gang Wang, Chunping Jiang, Jing Tian, Jinwei Chen and Ruilin Wang[1]

College of Materials Science and Engineering, Sichuan University, Chengdu, People's Republic of China

E-mail: rlwang26@yahoo.com.cn

Received 14 September 2012, in final form 1 November 2012
Published 10 December 2012
Online at stacks.iop.org/JPhysD/46/035103

Abstract

Beta-Bi_2O_3 film photoanodes with different surface structures were prepared by oxidizing bismuth films. The physical properties were characterized by x-ray diffraction (XRD), scanning electron microscopy (SEM), UV–visible absorbance spectra and atomic force microscopy (AFM). XRD shows that all films are beta phase crystal structure except the thinnest 12 nm film. SEM and AFM characterizations indicate that a nanoporous surface structure is generated on the surface after the film is annealed for 3 h, while the films annealed for 1 h show a dense surface. The direct band gaps vary from 2.63 to 2.88 eV, with the film thickness decreasing from 500 to 12 nm. The nanoporous surface structure film exhibits better light harvesting ability and incident photon-to-electron conversion efficiency (IPCE) than the dense surface films. The IPCE (61% at 350 nm and 43% at 400 nm, 0.197 V_{NHE}) is the highest ever reported. The photocurrent density reaches 0.45 mA cm^{-2} when illuminated with a bias of 1.23 V_{NHE} in 0.5M Na_2SO_3.

(Some figures may appear in colour only in the online journal)

1. Introduction

Direct photo-decomposition of water by semiconductor photocatalysts into hydrogen and oxygen is a promising way to produce clean and renewable energy. Since Fujishima and Honda [1] discovered the water splitting effect by illuminating a TiO_2 electrode under UV irradiation, a large number of studies have been carried out to find suitable materials. However, most of the experiments failed to obtain the conversion efficiency for commercial use. There were four essential requirements [2, 3] for the material to photo-decompose water into H_2 and O_2. In recent years, bismuth vanadate and bismuth tungstate, $BiVO_4$ [4] and Bi_2WO_6 [5], have been paid considerable attention in many studies. However, pure β-Bi_2O_3 is an important metal–oxide–semiconductor with a direct band gap of 2.8 eV. Its photocatalytic activity corresponds to visible light, [6, 7]. Due to the good charge mobility of β-Bi_2O_3, excited electrons and holes could have relatively long lives. Thus, they could be separated easily under specific conditions. The recombination inside the film could be reduced ultimately. So far, many different β-Bi_2O_3 photocatalysts have been reported. Harriman *et al* [8] prepared the solid solutions of Bi_2O_3 and Nb_2O_5 crystallize and the material could photo-decompose chlorinated hydrocarbons. Zhang *et al* [9] reported that sonochemically synthesized monoclinic nanocrystallite Bi_2O_3 (E_g = 2.85 eV) could degrade 86% of methyl orange within 100 min under visible light illumination. Kim *et al* [10] fabricated a β-Bi_2O_3 thin film on Au-coated Si substrates by means of metal organic chemical vapour deposition (MOCVD). A one-dimensional structure was formed at a low temperature of 400 °C with a diameter of about 30–90 nm. β-Bi_2O_3 nanofibres [11] were prepared by electro-spinning a precursor mixture of polyacrylonitrile/bismuth-nitrate and then annealing at different temperatures. The photo-activity was high for photo-degradation of Rhodamine B and the photo-activity did not decrease after illumination. Brezesinski *et al* [12] synthesized cubic mesoporous β-Bi_2O_3 thin films (E_g = 2.85 eV) by coassembly of hydrated bismuth nitrate with the poly-(ethylene-co-butylene)-block-poly(ethylene oxide) diblock copolymer. For improving the structural stability of β-Bi_2O_3, Wang *et al* [13] doped β-Bi_2O_3 with titanium by the hydrothermal method. After photo-degradation of

[1] Author to whom any correspondence should be addressed.

three kinds of dyes, the Ti-doped β-Bi_2O_3 was still chemical stable. Huang *et al* [5] compared the photo-activity between α-Bi_2O_3 and β-Bi_2O_3. The β-Bi_2O_3 showed narrower band gap with better light harvesting ability in the visible region, which resulted in a higher photocatalytic activity. Zhu *et al* [14] determined that 2.0 wt% Ag-doped β-Bi_2O_3 showed the best photo-activity by degradation of Rhodamine B. Ag/β-Bi_2O_3 structure was good for the migration of the electron–hole pairs, resulting in a higher visible light photocatalytic activity. Qiu *et al* [15] investigated the growth conditions of nanowires systematically. The β-Bi_2O_3 nanowires had better photo-degradation ability than α-Bi_2O_3. Moniz [16] reported that the β-Bi_2O_3 prepared by low-pressure chemical vapour deposition (LPCVD) had a band gap of about 2.3–3.0 eV. When illuminated, O_2 was oxidized from water and the calculated quantum yield efficiency (QE) was about 9.8% at 365 nm.

We mainly studied how the nanoporous surface structure affects the photo-activity in this experiment. The relationship between the film thickness and photoelectrochemical property was also assessed. We discovered that the photo-activity of the porous surface film was twice as high as the dense surface film. We also obtained the highest photon-to-electron conversion efficiency (IPCE) (61% at 350 nm and 43% at 400 nm, respectively) for β-Bi_2O_3 material.

2. Experiment

2.1. Thin film preparation

Bismuth films of different thicknesses were deposited by a radio frequency magnetron sputtering system on FTO conductive glass (TEC 15, 14 Ω/square, 25 × 25 mm^2). Pure bismuth (99.99%) was used as the sputtering target. One edge of the FTO surface was covered by a polyimide tape, which was used for the photoelectrochemical testing contact later. The base vacuum was 8.0×10^{-4} Pa, the argon flow was kept at 30 sccm, and the sputtering power was 20 W. The depositing time was 5 min (sample no 1), 40 min (sample no 2 and no 3) and 90 min (sample no 4), respectively (table 1). The 40 min sample was cut into two pieces and marked as sample no 2 and sample no 3. Sample no 1 and no 2 were annealed at 250 °C in air for 1 h to turn the metal into pure metal oxide. Sample no 3 and no 4 were annealed for 3 h at 250 °C in air to obtain the nanoporous surface structure.

2.2. Physical characterizations

Film thickness was measured by Alpha-Step D-100. The surface structure was characterized by an S-4800 scanning electron microscope and a CSPM-4000 model atomic force microscope. XRD was used to characterize the phase state in the scanning range 20°–70° (2θ) (Cu Kα_1 radiation, λ = 1.540 56 Å, 40 kV, 25 mA). UV–visible absorbance spectra were measured to study the light harvesting ability. Clean blank FTO glass was used as the standard baseline.

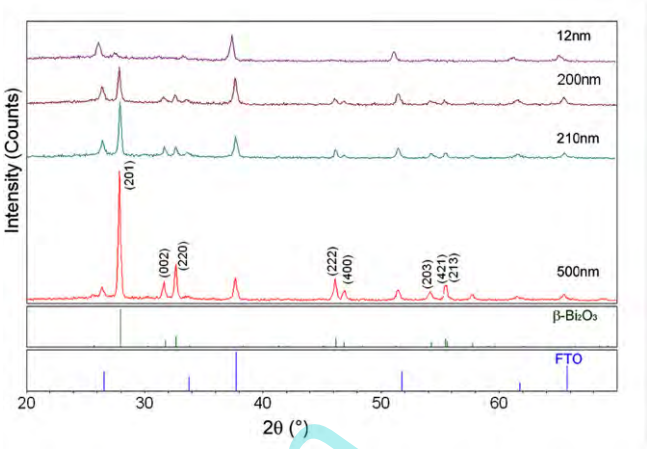

Figure 1. XRD patterns of β-Bi_2O_3 thin films.

2.3. IPCE and APCE measurements

The IPCE measurements were carried out in a self-made vessel fitted by quartz window in 1.0M NaOH solution. The system was made of an SBP500 monochromator, a potentiostat, a lock-in amplifier and one 150 W xenon lamp. A graphite rod was used as the counter electrode, and Ag/AgCl (saturated KCl solution) as the reference electrode in all experiments. The relationship between NHE and the Ag/AgCl reference electrode is $E_{NHE} = E_{Ag/AgCl} + 0.197$ V [17].

2.4. Photocurrent test

The photocurrent data were collected by solartron 1287 and 1260 electrochemical interface in 0.5M Na_2SO_3 solution. Illuminating light source was a 150 xenon lamp with an AM 1.5 filter. The light intensity was 60 mW cm^{-2} measured by a sun meter.

3. Results and discussion

3.1. X-ray diffraction

XRD was used to identify the crystal phase of samples. Figure 1 reveals that all films exhibit pure β-phase except the 12 nm film (tetragonal, JCPDS card No 27-0050) and there are no other phases (α- or δ- Bi_2O_3). The (2 0 1) peak position of the 12 nm sample is varied from the standard (2 0 1) line,

The diffraction density becomes stronger with increasing film thickness. The thinnest 12 nm film shows a weak (2 0 1) peak and there are no obvious diffraction peaks of β-Bi_2O_3, while the other three films have good crystallinity after annealing. The samples exhibit pre-orientation in the (2 0 1) direction. The calculated unit cell dimensions of $a = b = 7.7$ Å and $c = 5.7$ Å are in agreement with reference values ($a = b = 7.741$ Å, $c = 5.634$ Å) [18]. The grain size of the film is calculated by Debye–Scherrer's formula [19, 20]:

$$D = \frac{K\lambda}{(\beta \cos\theta)},$$

where D is the crystallite mean dimension, K is the Scherrer constant ($K = 0.94$), λ is the wavelength of Cu Kα_1, β is

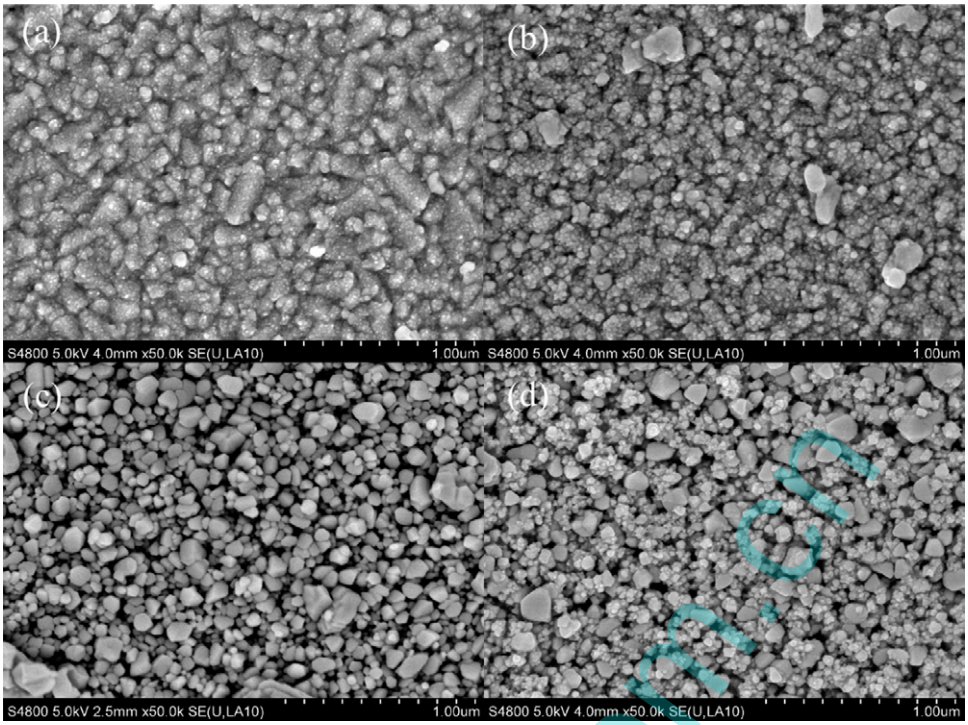

Figure 2. SEM images of β-Bi_2O_3 thin films: (*a*) 12 nm, dense surface; (*b*) 200 nm, dense surface; (*c*) 210 nm, nanoporous surface; (*d*) 500 nm, nanoporous surface with accumulated tiny grains. Length scale: 1μm.

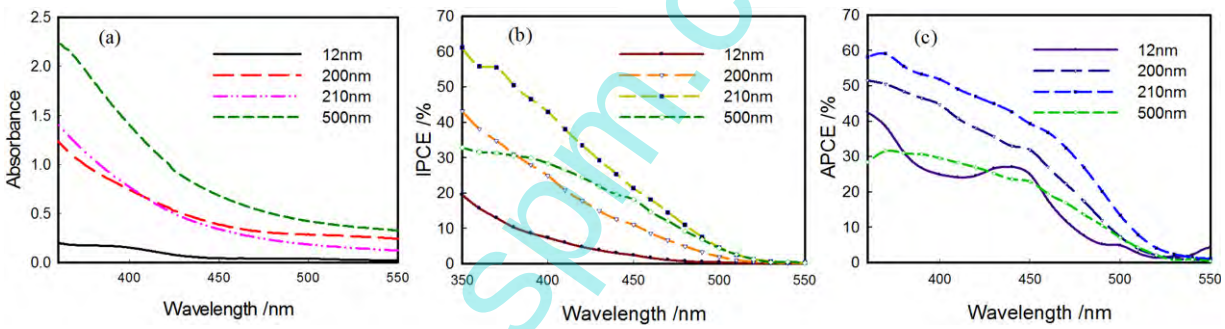

Figure 3. UV–visible absorption spectra (*a*), IPCE (*b*) and APCE (*c*) of β-Bi_2O_3 films.

the full-width at half-maximum and θ is the Bragg diffraction angle. The calculation is based on the (2 0 1) peak. The estimated grain sizes are listed in table 1.

3.2. Surface morphology

The surface structures of the four samples are shown in figure 2. The 12 nm film (figure 2(*a*)) shows a densely arranged surface and the particles grow on the surface of SnO_2, so it is difficult to identify the grain size from XRD data. A large number of nano-polygon particles (50–150 nm) are formed on the other three film surfaces. As the film thickness increases, tiny grains aggregates with each other and finally form bigger particles. There is a lot of empty space among those particles in figures 2(*c*) and (*d*). But figure 2(*c*) has better crystallinity than figure 2(*d*), because there are many tiny particles accumulated around bigger particles on the surface accompanied by more drawbacks. Figures 2(*b*) and (*c*) were made from the same bismuth sample but the annealing time was different. So the porous surface was generated during the annealing process.

Many small crystal particles are formed enclosing larger particles in figure 2(*d*). The reason may be that there is inadequate annealing time for the grains to grow into large crystals. Figure 2(*b*) shows that the surface structure of the 200 nm sample (annealed for 1 h) is a dense surface. The nanoporous surface structure enables the electrolyte to permeate into the surface, reacting with the photogenerated holes directly on the particle surface. So, the porous surface could potentially promote the charge transfer process [21–23, and eventually increase PEC efficiency.

3.3. UV–visible absorbance spectra

The UV–visible absorbance spectra of each sample are shown in figure 3. The derived energy gap of the β-Bi_2O_3 films are based on the Tauc formula (figure 4) [24, 25]:

$$(\eta h\upsilon)^2 \propto A(h\upsilon - E_g).$$

Table 1. Physical properties of Bi_2O_3 films.

Sample no	Annealing time (h)	Thickness (nm)	(2 0 1) FWHM (°)	Grain size (nm)	E_g (eV)	Surface structure
1	1	12	Undefined	Undefined	2.88 ± 0.02	Dense
2	1	200	0.205	45	2.83 ± 0.03	Dense
3	3	210	0.204	44	2.75 ± 0.02	Porous
4	3	500	0.186	48	2.63 ± 0.02	Porous

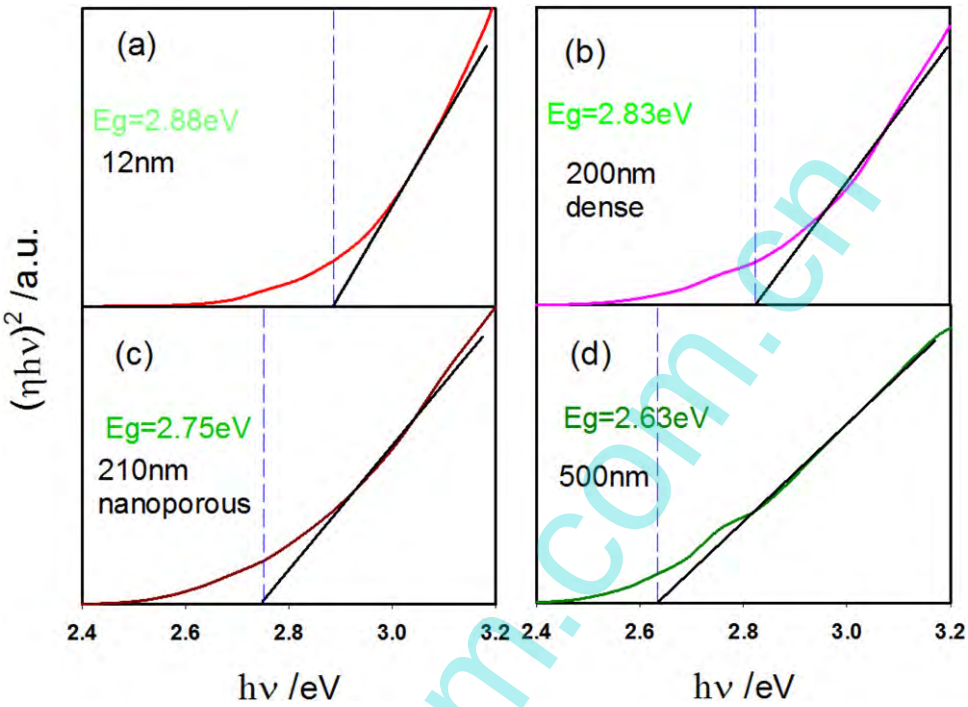

Figure 4. Direct band transition fitting versus photon energy of β-Bi_2O_3 thin films: (*a*) 12 nm film, (*b*) 200 nm dense film, (*c*) 210 nm nanoporous film, (*d*) 500 nm film.

Here, the quantum efficiency, η, is proportional to the square root of the photon energy under direct transition condition. A is the proportionality constant, $h\nu$ is the photon energy and E_g is the energy gap. The calculated energy gap is listed in table 1.

The direct energy gaps of the four samples are in accordance with George's report [26] but narrower than the β-Bi_2O_3 nanowires reported [12]. Figure 4 indicates that the band gap decreases with increasing film thickness. The 12 nm film has the widest energy gap of 2.88 eV because of its nanosize effect. The nanoporous surface film shows better photo-absorbance and narrower E_g than those of the dense surface film, because the empty space on its surface could reflect the incident light and then the adjacent particles can absorb the reflected light, which improves the light absorbing process eventually (figure 5(*d*)). As a visible light photocatalyst candidate, the 500 nm film extends the absorbance edge to 470 nm, which means it could utilize more sunlight.

3.4. IPCE and APCE

The induced IPCE is defined as

$$\mathrm{IPCE} = \frac{I}{P}\frac{1240}{\lambda} \times 100\%,$$

where I is the photocurrent density (mA cm^{-2}). P is the power of the monochromatic light irradiated on the electrode (mW cm^{-2}) and λ is the wavelength (nm). The measurements are carried out under $0.197\mathrm{V}_{\mathrm{NHE}}$ (figure 3(*b*)). All films exhibit good photo-activity in the visible light region ($\lambda \geqslant 400$ nm). The 210 nm film exhibits the highest IPCE at 350 nm and 400 nm, which is 61% and 43%, respectively. The IPCE of the 210 nm sample is almost six times that of the reported bismuth oxide thin films prepared by MOCVD [16]. β-phase Bi_2O_3 has an intermediate conductivity between the α- and δ-phase. So there are three advantages for the 210 nm nanoporous film. First, it has a narrow energy gap of about 2.73 eV, which means it could harvest more visible light photons than the thinner sample and ultimately induce more electrons and holes. Second, it shows the best crystallinity among the four samples, which contributes to its conductivity. Most of the photogenerated electrons could move to the back contact electrode (FTO) rather than recombining with holes in the bulk film and hence reduce the recombination inside the film. Since the particles in the 200 nm films are not as big as the particles in the 210 nm film, the photoelectrochemical performance of the 200 nm film is lower than that of the 210 nm one. Although the 500 nm film had better light absorption ability, it could not obtain better photoelectrochemical performance

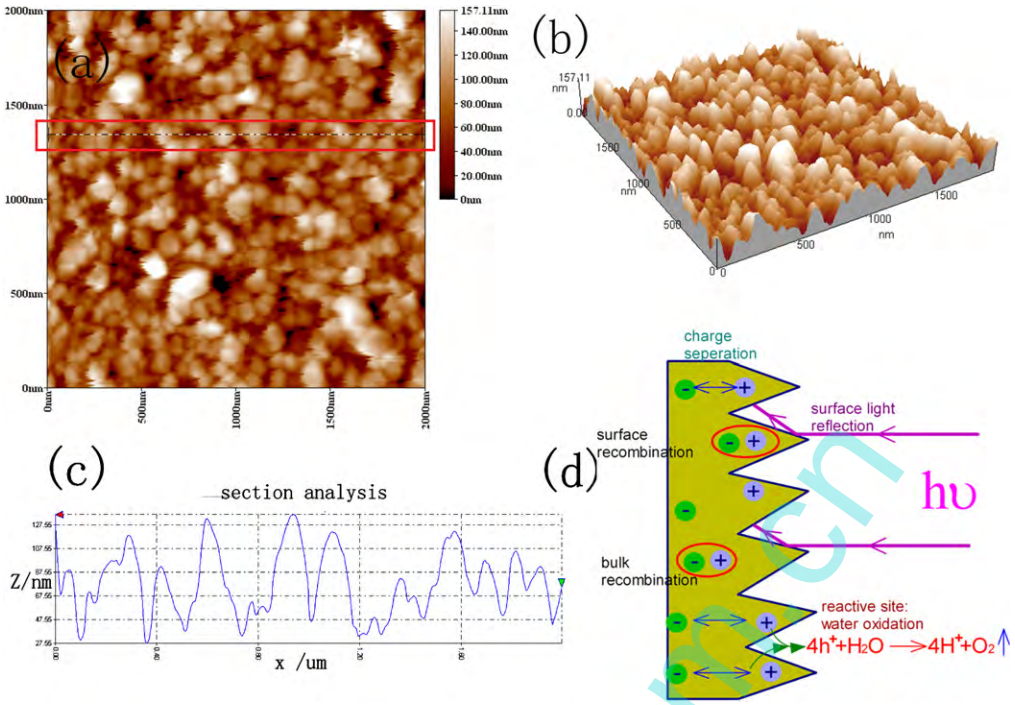

Figure 5. AFM surface structure (*a*), three-dimensional image (*b*), section analysis (*c*) and Schematic diagram of the photoelectrochemical processes (*d*) in the 210 nm nanoporous surface film.

than the 210 nm film, owing to its surface defects. Third, the nanoporous surface structure of the 210 nm film allows the electrolyte to permeate to the empty space among the particles and enlarge the contact area between particles and electrolyte. Therefore, photogenerated holes on the surface could react with OH^- ions in the electrolyte directly, which also finally reduced the recombination on the surface. Figures 5(*a*), (*b*) and (*c*) show the surface structure, three-dimensional surface and section analysis of the red rectangle marked area of the 210 nm film. The surface structure analysis conforms to the former assumptions.

Some researchers had also fabricated β-Bi_2O_3 thin films; however, most of them failed to contain the three advantages at the same time. So the photoelectrochemical performance was not as ideal as the samples in this experiment. Based on Hameed's [27] work, the 210 nm film may be a composite of Bi_2O_3 and Bi_2O_{4-x}. Among all the oxidizing species, superoxide radical has the highest oxidation power and the sufficiently long lifetime. So the photogenerated holes on the film surface could live long and then move to the reactive site on the surface. The photocurrent density is shown in figures 6(*a*) and (*b*). Here the onset potential of all the films is located at $-0.15V_{NHE}$, in 0.5M Na_2SO_3 solution. The photocurrent density of nanoporous 210 nm film reaches 0.45 mA cm^{-2} under $1.23V_{NHE}$, while that of the 200 nm film with dense surface reaches only 0.04 mA cm^{-2} at $1.23V_{NHE}$. So the photoelectrochemical property is increased strongly by the nanoporous structure.

The absorbed photon-to-current efficiency (APCE) of the four samples is shown in figure 3(*c*). APCE is defined by the formula [10]

$$\mathrm{APCE} = \frac{\mathrm{IPCE}}{1 - 10^{-A}}.$$

Here A is the absorbance. $(1 - 10^{-A})$ represents the light harvesting efficiency (LHE) of the film. Owing to the nanoporous surface structure, the light is reflected between the crystal grains and the electrolyte on the surface rather than passing through the film directly on the dense film surface, which could relatively enlarge the photon absorbing ability. And the 210 nm film still possesses the highest APCE. The IPCE of the 12 nm film is 20% at 350 nm; however, the APCE is 30%, so more than half of the light is wasted when the light passes through the film. The 200 nm film with a dense surface shows smaller absorbance than the 210 nm film with a nanoporous surface. The 500 nm film is very thick, so the photogenerated electrons and holes cannot have enough time to pass through the film bulk and ultimately recombine with each other in the film. The APCE curve of 210 nm film decays smoothly ($\lambda < 450$ nm), which suggests that it has the best thickness among four films.

4. Conclusions

A series of highly photoactive β-Bi_2O_3 films were fabricated on FTO substrates. A β-Bi_2O_3 film with a nanoporous surface structure is generated by prolonging the annealing time. The particle size of the 210 nm film is bigger than the other three films, and there are fewer small particles generated on the surface than the thick 500 nm film. The prepared films with varied thickness show different photo-response and photoelectrochemical performance. IPCE and APCE analyses indicate that the 210 nm film with a nanoporous surface shows the highest photoelectrochemical activity at a bias of $0.197V_{NHE}$, because it possesses three advantages (effective light harvesting ability, good crystallinity and nanoporous

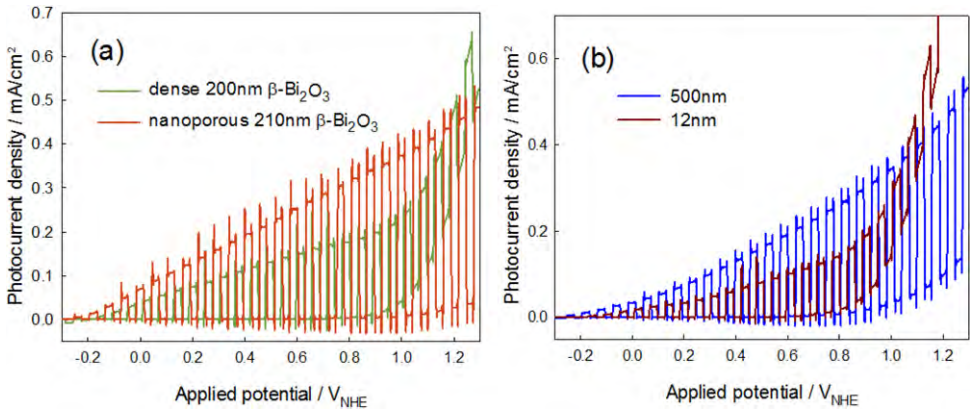

Figure 6. *I*–*V* plots of dense 200 nm surface and 210 nm nanoporous surface films (*a*); dense surface 12 and 500 nm films (*b*).

surface structure) to reduce bulk and surface recombination at the same time. From the comparison with dense and nanoporous surface structures, we discover that the nanoporous surface could promote the photoelectrochemical property of β-Bi_2O_3 strongly.

Acknowledgments

This work is supported by the 863 project (2006AA05Z102) and the Specialized Research Fund for the Doctoral Program of Higher Education (20110181110003).

References

[1] Fujishima A and Honda K 1972 *Nature* **238** 37–8
[2] Chen X B, Shen S H, Guo L J and Mao S S 2010 *Chem. Rev.* **110** 6503–70
[3] Lian X, Yang X, Liu S, Xu Y, Jiang C, Chen J and Wang R 2012 *Appl. Surf. Sci.* **258** 2307–11
[4] Iwase A and Kudo A 2010 *J. Mater. Chem.* **20** 7536–42
[5] Huang Q Q, Zhang S N, Cai C X and Zhou B 2011 *Mater. Lett.* **65** 988–90
[6] Maruthamuthu P, Gurunathan K, Subramanian E and Sastri M V C 1993 *Int. J. Hydrogen Energy* **18** 9–13
[7] Maruthamuthu P, Gurunathan K, Subramanian E and Sastri M V C 1994 *Int. J. Hydrogen Energy* **19** 889–93
[8] Harriman A, Thomas J M, Zhou W and Jefferson D A 1988 *J. Solid State Chem.* **72** 126–30
[9] Zhang L S, Wang W Z, Yang J O, Chen Z G, Zhang W Q, Zhou L and Liu S W 2006 *Appl. Catal.* A **308** 105–10
[10] Kim H W, Lee J W, Shim S H, Kebede M A and Lee C 2008 *Cryst. Res. Technol.* **43** 695–9
[11] Wang C H, Shao C L, Wang L J, Zhang L, Li X H and Liu Y C 2009 *J. Colloid Interfce Sci.* **333** 242–8
[12] Brezesinski K, Ostermann R, Hartmann P, Perlich J and Brezesinski T 2010 *Chem. Mater.* **22** 3079–85
[13] Wang Y, Wen Y Y, Ding H M and Shan Y K 2010 *J. Mater. Sci.* **45** 1385–92
[14] Zhu G Q, Que W X and Zhang J 2011 *J. Alloys Compounds* **509** 9479–86
[15] Qiu Y F, Yang M L, Fan H B, Zuo Y Z, Shao Y Y, Xu Y J, Yang X X and Yang S H 2011 *Crystengcomm* **13** 1843–50
[16] Moniz S J A, Blackman C S, Carmalt C J and Hyett G 2010 *J. Mater. Chem.* **20** 7881–6
[17] Reece S Y, Hamel J A, Sung K, Jarvi T D, Esswein A J, Pijpers J J H and Nocera D G 2011 *Science* **334** 645–8
[18] Blower S K and Greaves C 1988 *Acta Crystallogr.* C **44** 587–9
[19] Patterson A L 1939 *Phys. Rev* **56** 978–82
[20] Gariné G, Fernando E, Carlos J P, Ricardo E M, Francisco M, Dietmar L, José R R-B and Enrique A D 2012 *J. Phy. D: App Phys.* **45** 245301
[21] Aroutiounian V M, Arakelyan V M and Shahnazaryan G E 2005 *Sol. Energy* **78** 581–92
[22] Perez M A and Teijelo M L 2005 *J. Electroanal. Chem.* **583** 212–20
[23] Wu Z F, Huang F Z, Shen Y H, Xie A J and Song X Q 2011 *J. Nanopart. Res.* **13** 4575–82
[24] Tauc J 1967 *Science* **158** 1543–8
[25] Shaban Y A and Khan S U M 2008 *Int. J. Hydrogen Energy* **33** 1118–26
[26] George J, Pradeep B and Joseph K S 1987 *Phys. Status Solidi* a **103** 607–12
[27] Hameed A, Montini T, Gombac V and Fornasiero P 2008 *J. Am. Chem. Soc.* **130** 9658–9